Direct Simulation Monte Carlo Analysis of Flow in Knudsen Pumps with Square-Shaped Wall Roughness

N. Mirnezhad, A. Amiri-Jaghargh*, A. Qaderi

Department of Mechanical Engineering, Razi University, Kermanshah, Iran

ABSTRACT: Thermal creep Knudsen pumps are made up of micro/nanochannels subjected to a temperature gradient. In such a combination, the fluid flows from the cold side to the hot side based on the thermal creep phenomenon. Due to the widespread use of Knudsen pumps in various applications, much research has been done to improve their technology. In this work, the effects of wall surface roughness on the flow field characteristics are investigated using the molecular-based direct simulation Monte Carlo method. The surface roughness is modeled by square bumps on the wall. The roughness parameters, including relative roughness, roughness aspect ratio, and roughness distance, are studied in a wide range, that is, $0 \leq \varepsilon \leq 10$, $0.5 \leq \xi \leq 2$, and $3 \leq \chi \leq 10$, respectively. It is concluded that the existence of roughness, no matter how small, has a significant effect on the flow conditions; so that the subminiature roughness of $\varepsilon = 0.5\%$ results in a 24% decrease in the mass flow rate. This emphasizes the importance of considering the role of surface roughness in the calculation of the performance of Knudsen pumps. Furthermore, the results indicate that the mass flow rate is independent of the relative roughness and the roughness distance for $\varepsilon \leq 1.25\%$ and $\chi \leq 5$, respectively

1- Introduction

Knudsen pumps are one of the interesting devices constructed using Micro-Electromechanical Systems (MEMS) technology. The most attractive feature of Knudsen pumps, in contrast to mechanical pumps, is that they work based on the thermal transpiration phenomenon, and so have no moving part. When the thermal gradient is applied along a wall, a flow appears in the gaseous layers adjacent to the wall from the cold side to the hot side, which is known as thermal creep flow [1]. Simple structure, less repair and maintenance costs, good performance concerning their dimensions, more uniform flow, and economic feasibility are the other advantages of Knudsen pumps over their mechanical counterparts.

There are many studies concerning the Knudsen pump applications and their working conditions. Vargo and Muntz [2] constructed the first Knudsen pump operating in atmospheric pressure. That pump could only produce a 1.5 kPa pressure difference, however, the pumping ability can be improved by using multistage structures. Gupta and Gianchandani [3] proposed multistage Knudsen pumps for the first time, by fabricating a 9-stage Knudsen pump from nanoporous ceramic material. It was able to create a maximum 12 kPa pressure gradient and a 3.68 μlit∕min volume flow rate at 160 Pa pressure. Thanks to the novel fabrication techniques, the multistage Knudsen pumps have much better performance nowadays. Toan et al. [4] fabricated a Knudsen pump with 96 hot and cold chambers that were capable to decrease the atmospheric pressure to about 10 kPa. To predict the performance of multistage Knudsen pumps, Kugimoto et al. [5] suggested a two-step numerical-experimental method. The method included a 1D model for multistage Knudsen pumps, which was adjusted based on experimental results of the one-stage pump. Ye et al. [6] established a numerical model of multistage hydrogen Knudsen pumps. They showed for a small number of stages, the compression ratio has a linear relation with stage number.

The microchannel structure can also affect the performance of Knudsen pumps. Aoki et al. [7] proposed a Knudsen pump that utilizes curved channels. They used the Direct Simulation Monte Carlo (DSMC) method and showed that 2D snaky cascade geometry could produce a significant compression ratio. Bond et al. [8] investigated the thermal creep phenomenon in the Knudsen pumps with double curved channels. Their results showed that S-shaped geometry leads to an improvement of more than 100% in mass flow rate. In more recent work, they considered the sinusoidal structure as well [9]. The study of tapered Knudsen pumps [10, 11] demonstrates a significant decrease of flow rate with increasing inclination angle. Diverging channel Knudsen pumps have a larger mass flow rate with respect to converging channels.

*Corresponding author's email: amirij@gmail.com

Besides the shape of the channels, surface attributes such as wall roughness affect the flow field features in microflows. Cao et al. [12] simulated the slip flow of gaseous argon inside platinum microchannels with different shapes of submicron roughness. They concluded that friction coefficient increases not only with decreasing the Knudsen number but also with increasing the surface roughness. Zhang et al. [13] used the lattice-Boltzmann method for simulating the gaseous slip flow inside the microchannels with rough surfaces. Their results showed that the wall roughness reduces the slip velocity. It was also revealed that decreasing the height of the roughness as well as increasing the Knudsen number leads to significant slip velocity on the microchannel walls. Rovenskaya and Croce [14] investigated fluid flow inside a rough microchannel using dynamic coupling between the kinetic and Navier-Stokes equations. The roughness was modeled by triangular elements with a maximum relative roughness of 5%. The effect of the roughness height on the Poiseuille number and the mass flow rate were studied. The results showed that the roughness increases the Poiseuille number and decreases the mass flow rate. They also concluded that the more dilute the gas is, the more intense the effect of roughness is. Jia et al. [15] investigated the effect of wall roughness on the fluid flow and heat transfer of the low Reynolds flows in microchannels. They used a fractal structure to simulate the roughness. Their results showed that increasing the surface roughness increases both the heat transfer performance and friction coefficient.

It should be noted that the origin of the flow in Knudsen pumps is thermal creep which is a gas-surface interaction phenomenon. Therefore, the surface roughness may have different effects in comparison to pressure-driven flows that have been reviewed so far. For a comprehensive review of the Knudsen pumps, see the recent study of Wang et al. [16] where no investigation on the surface roughness in Knudsen pump flow is mentioned. Yamamoto et al. [17] used a linearized B-G-K equation to simulate thermal creep flow between two parallel plates with surface grooves parallel and/or perpendicular to the flow direction. They showed that even shallow grooves lead to a significant reduction in mass flow rate. Shao et al. [18] simulated a Knudsen pump with a rectangular and/or triangular obstacle in the microchannel. In their other work, Ye et al. [19] investigated a semicircular obstacle. They demonstrated that the Knudsen pump pressure ratio can be increased by increasing the width of the obstacles whereas it decreases as the height of the obstacles increases.

The survey of the available literature indicates a lack of information on the subject of thermal creep flow in rough channels. The effects of roughness parameters such as relative roughness, aspect ratio, and the distance between roughness elements on the key features of thermal creep flow, are not been investigated in detail so far. In our recent work [20], we examined the effects of triangular shaped rough elements on the critical parameters of thermally-driven flow in microchannels. But, micro/nano flows have memory which means that the flow depends on the details of roughness [21]. So, to have a conclusive view of the roughness, other protrusion shapes should also be studied. Therefore, in the present study, the roughness is modeled by square elements on the wall where a linear temperature gradient is applied to induce the thermal creep flow. A square protrusion has a side parallel to the core flow and so is basically different with triangular roughness. The DSMC method is utilized to simulate thermal creep flow. In this method, the thermal creep phenomenon is simulated by following the motion of the molecules, and no mathematical model is employed. Thus, it is an accurate way to simulate the flow in Knudsen pumps, especially in the transient flow regime.

2- Model Description

The thermal creep Knudsen pump is made up of microchannels with two cold and hot ends. Therefore, to study the effects of roughness on the flow in the Knudsen pump, it is sufficient to consider one of these microchannels with a temperature gradient along the wall. In this study, the thermal creep flow inside the planar microchannel of 1.2×0.2 μm with square roughness on the walls is investigated. Fig. 1 shows a schematic view of the channel, roughness parameters, and the applied boundary conditions.

Knudsen pumps usually work in a transient flow regime ($0.1 < Kn < 10$). Thus, the inlet Knudsen number, which is calculated based on the channel height ($2H$), is assumed to be $Kn = 1$ in all cases where the effects of roughness are investigated. The inlet pressure is $P_{in} = 26806.362$ Pa which is calculated based on the inlet Knudsen number. It is worth mentioning that the outlet pressure is assumed to equal the inlet pressure to make sure that the thermal gradient on the walls is the only factor that induces flow in the microchannel.

The temperature of the channel walls changes linearly from 300 K at the inlet to 400 K at the outlet. The inlet gas temperature is adjusted at 300 K. The diatomic Nitrogen, $m = 4.65 \times 10^{-26}$ kg, and $d = 4.17 \times 10^{-10}$ m is considered as a gaseous medium. Regarding the symmetry of the channel and the boundary conditions, the only upper half of the channel is simulated. Consequently, the symmetry boundary condition is applied on the lower boundary.

The roughness parameters depicted in Fig. 1 are a, b, and c, which stand for height, length, and the step of the roughness elements, respectively. The dimensionless forms of the roughness parameters are defined as relative roughness, $\varepsilon = a / 2H$, roughness aspect ratio, $\xi = b / a$, and the relative roughness distance (in summary called roughness distance), $\chi = c / a$. To investigate the effects of wall roughness, these parameters are considered to vary in wide ranges, that is $0 \leq \varepsilon \leq 10$, $0.5 \leq \xi \leq 2$ and $3 \leq \chi \leq 10$.

3- Numerical Method

The Direct Simulation Monte Carlo (DSMC) method is used to simulate the thermally-driven flow. DSMC is a particle-based method where each particle represents a large number of molecules (f_{num}). The main feature of DSMC is that the motion of the particles is decomposed into two parts of movement and collision. During each time step, particles move based on Newton's second law of motion. Then, the
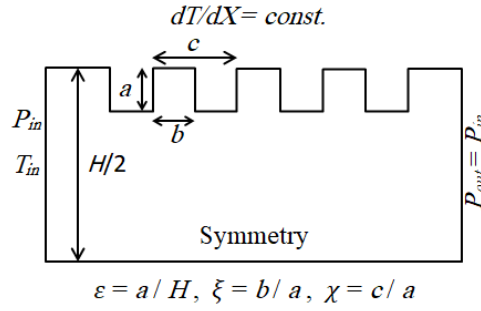
$$\varepsilon = a / H, \; \xi = b / a, \; \chi = c / a$$

Fig. 1. Schematic representation of the channel and the boundary conditions

collision is modeled by a velocity change of colliding particles. The collision is assumed to be binary, which is accurate enough for dilute gases. Provided that the method constraints, such as time step, computational cell size, and the number of particles per cell are satisfied, it is mathematically proved that the DSMC method matches the results of the Boltzmann equation [22]. To implement the DSMC procedure, the domain must be divided into computational cells where the collisional pairs are selected. This also provides a framework to sample the thermophysical properties. The collisional pairs are selected by the No Time Counter (NTC) scheme [23]. In this scheme, first, the number of collisions (N_c) that should happen in the computational cell l, is evaluated from,

$$N_c = \frac{1}{2} f_{num} N^l \left\langle N^l \right\rangle \left(\sigma g\right)^l_{max} \Delta t / \forall^l \tag{1}$$

where f_{num}, $\left(\sigma g\right)^l_{max}$ and $\forall$ are the ratio of the number of real molecules to simulated particles, maximum of collision cross-section multiplied by particles' relative velocity and cell volume, respectively. Then a random pair of particles are selected and checked for a possible collision with the probability of,

$$\mathrm{p}_{ij} = \frac{\sigma_{ij} g_{ij}}{\left(\sigma g\right)_{max}} \tag{2}$$

where σ_{ij} and g_{ij} are the effective collision cross-section and the magnitude of the relative velocity of the pair (i, j). If the particles are accepted for collision through an acceptance-rejection procedure, the particles' velocities are updated based on the elastic collision formula.

$$u_r^* = \cos \chi u_r + \sin \chi \cos \varepsilon \left(v_r^2 + w_r^2\right)^{1/2}$$

$$v_r^* = \cos \chi v_r +$$
$$\quad \sin \chi \left(c_r w_r \cos \varepsilon - u_r v_r \sin \varepsilon\right) / \left(v_r^2 + w_r^2\right)^{1/2} \tag{3}$$

$$w_r^* = \cos \chi w_r +$$
$$\quad \sin \chi \left(c_r v_r \cos \varepsilon - u_r w_r \sin \varepsilon\right) / \left(v_r^2 + w_r^2\right)^{1/2}$$

where $u_r v_r w_r$ is the particles relative velocity before the collision and the superscript $*$ refers to after collision relative velocity components. With updated velocities, particles are ready to move in the next time step and all the procedures will be repeated until steady-state results are achieved. More details of the DSMC method are described in [23-25]. An improved version of OpenFOAM based DSMC solver named dsmcFoamStrath is utilized to solve the problem. In which, the Variable Hard Sphere (VHS) model and the NTC scheme are used for binary collision model and collision partner selection scheme, respectively.

3- 1- Validation

To validate the results, some benchmark cases are solved and compared with the data in the literature. Thermally-driven flow in Knudsen pumps is somehow similar to shear-driven flow in which the fluid motion originates from the wall. Therefore, a Couette flow studied by Liou and Fang [26] is considered as the first case of validation. In this simulation, the Knudsen number, inlet, and outlet pressures, inlet and wall temperatures, and the driving wall velocity were $Kn = 0.08$, $P_{in} = P_e = 0.83$ atm, $T_{in} = T_w = 300$K, and $U_w = 100$ m/s, respectively. Fig. 2 shows the velocity profiles from dsmcFoamStrath solver and Liou and Fang work; there is a good agreement between the results, so that the average
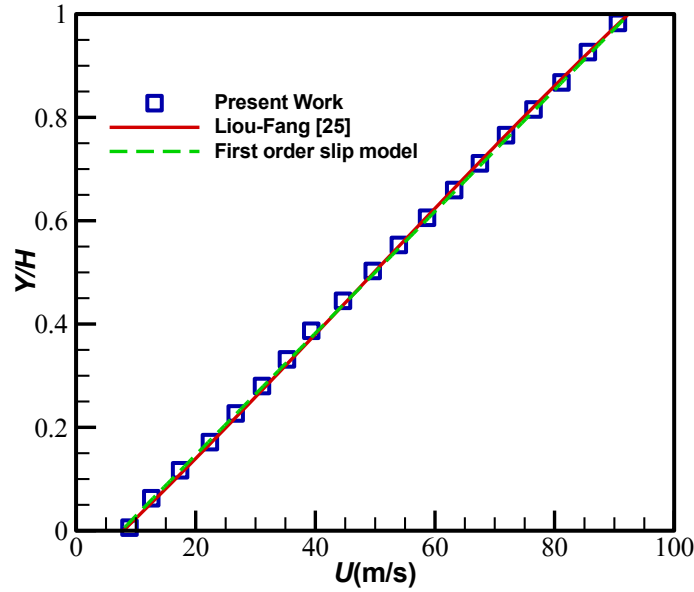
Fig. 2. Comparison of the velocity profiles with Liou and Fang work [26]

and maximum errors are 1.25% and 3.5%, respectively. Since the flow falls in the slip flow regime ($Kn \leq 0.1$), the results are compared to the analytical solution of Navier-Stokes equations accompanied with slip boundary condition, as well. For fully developed low Reynolds flow between parallel plates with no pressure gradient, the Navier-Stokes equations can be simplified to,

$$\frac{d^2U}{dY^2} = 0 \qquad (4)$$

The first order Maxwell slip boundary condition may be written as,

$$U - U_w = C_1 Kn \frac{dU}{dY}\bigg|_w \qquad (5)$$

Ohwada et al. [27] developed an analytical solution for linearized Boltzmann equation in Couette flow and showed $C_1 = 1.111$ predicts accurate results for $Kn \leq 0.1$. Integrating Eq. (4) with first-order slip boundary condition Eq. (5), the velocity profile becomes,

$$U = \frac{U_w}{1 + 2C_1 Kn}\left(\frac{Y}{H} + C_1 Kn\right) \qquad (6)$$

where $H = 0.8$ μm/s is the distance between the plates. Our DSMC result is compared with this analytical solution in Fig. 2 where a good agreement is shown with an average error of 1.2%. A maximum error of 9.9% appears near the stationary plate which is due to the weakness of continuum based analytical solution in the prediction of velocity profile in the Knudsen layer.

The ability of the solver in the prediction of mass flow rate is evaluated by comparing with the results of Akhlaghi and Roohi [28], where thermal creep flow in a smooth channel is simulated by the DSMC method using Bird's DSMC2 code. A linear temperature gradient of 50 K/μm was applied along the channel walls. Nondimensional mass flow rates are reported in Table 1 for modified Knudsen numbers of $Kn_{in} = 1$ and $Kn_{in} = 0.2$. According to this table, it can be observed that there is a good agreement between the results.

3- 2- Verification

After validating the solver, the independence of the results from the numerical parameters of the DSMC method is considered in this part. The main parameters which influence the results in the DSMC method are computational cell size, number of particles per cell, and time step. A straight smooth channel of 1.2×0.2 μm with inlet Knudsen number of $Kn_{in} = 0.25$ and temperature difference of 100 K on the walls is considered to simulate the thermal creep phenomenon. The inlet temperature is 300 K, and an equal pressure value of 0.83 atm is applied at both channel inlet and outlet.

To simulate the collision correctly, the computational domain should be divided into small enough cells that restrict

Table 1. Comparison of nondimensionalized mass flow rate

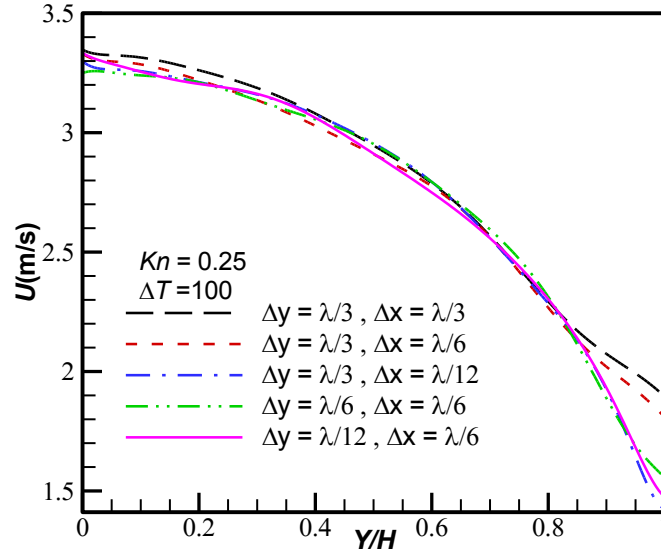|	$Kn_{in} = 0.2$	$Kn_{in} = 1$
Akhlaghi and Roohi [28]	0.0914	0.205
Present Work	0.0897	0.199
Error (%)	1.86	2.93

Fig. 3. Velocity profile at the $x / L = 0.5$ cross-section for various grids

the selection of colliding partners to the adjacent particles. Alexander et al. [29] showed that using a coarse grid leads to a 15% error in the prediction of viscosity, while the error decreases to 1% with reducing the cell size to $\Delta x \cong \lambda / 3$. Therefore, cell size is set to be $\Delta x = \Delta y = \lambda / 3$ as the first estimate, then finer grids of $\lambda / 6$ and $\lambda / 12$ are checked as well to ensure the results are independent of cell size. Fig. 3 shows the grid study results for the velocity profile at the $x / L = 0.5$ cross-section.

According to this figure, the grid with $\Delta x = \Delta y = \lambda / 6$ corresponding to 1728 cells in the domain and grid with $\Delta x = \lambda / 6$ and $\Delta y = \lambda / 12$ corresponds to 3456 cells are coincident with average and maximum errors of 1.02% and 2.4%, respectively. Therefore, the grid with $\Delta x = \Delta y = \lambda / 6$ is chosen to reduce the computational costs. It is worth mentioning that finer grids may be used for rough microchannels, especially at the corners of roughness elements.

The number of particles in each cell is the next parameter that should be evaluated. Previous studies showed that in the NTC scheme, it is enough to use 20 particles per cell [24]. Checking various numbers of particles per cell in this study leads to the same conclusion. Therefore, this study is done using 20 particles per cell.

The time step is the last factor which is verified to ensure the accuracy of the implementation of the DSMC method. It should be smaller than $1/3$ of average collision time [30], that is the time a molecule travels the average distance between two sequential collisions (λ) with the most probable speed $V_{mp} = \sqrt{2KT / m}$. Therefore, the first criterion on the time step is $\Delta t \leq \lambda / \sqrt{2RT}$. On the other hand, it should be noticed that the time step neither should be too large so that the particle leaves the cell after a time step nor be too small so that the particle remains in the cell after several time steps. Both of these conditions can cause an error in the results obtained from the DSMC method; consequently, another criterion for the time step is $\Delta t < \Delta x / 2\sqrt{2RT}$. Of these criteria, the smallest value is selected as the final time step that equals 1×10^{-11} s for this work. But to ensure the proper time step is selected, two other time steps are also checked. Fig. 4 shows the variation of the x-velocity component along the channel at $y / H = 0.75$ for various time steps. According to this figure, it is obvious that the results of time step 5×10^{-12} s lie excellently on the results of time step 1×10^{-11} s, so that the average and maximum errors are 0.67% and 1.82%, respectively. Therefore, the time step is set to be 1×10^{-11} s;
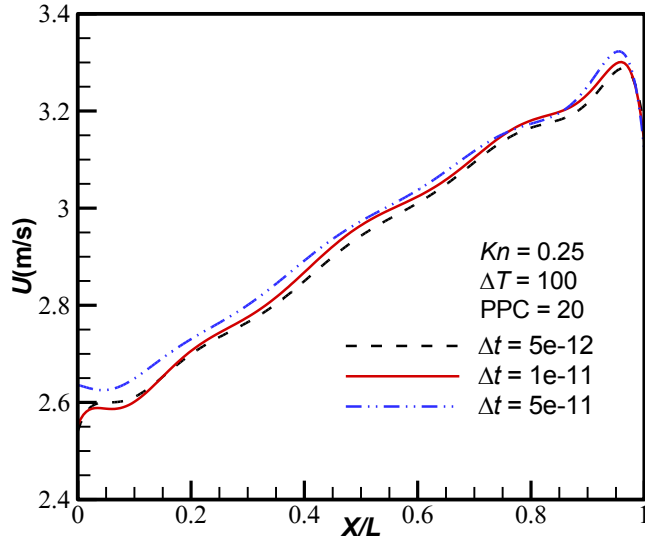
Fig. 4. Streamwise velocity component along the channel at $y/H = 0.75$ **for various time steps**
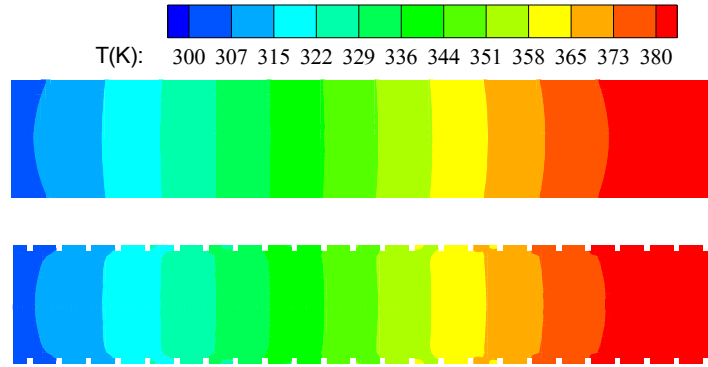

Fig. 5. Temperature distribution in smooth and rough microchannels

however, due to the dependency of time step on the grid size, based on the situation, a smaller time step may be used.

4- Results and Discussion

In order to simulate the roughness, the square elements are added to the channel walls, as described in section 2. The inlet Knudsen number is set to be $Kn = 1$ for all cases. The diatomic Nitrogen, $m = 4.65 \times 10^{-26}$ kg, and $d = 4.17 \times 10^{-10}$ m is considered as a gaseous medium. In Fig. 5, the temperature contours of smooth and rough channels are compared. The roughness parameters are $\chi = 5$, $\xi = 1$, and $\varepsilon = 5\%$. The figure demonstrates that the existence of the roughness does not significantly change the temperature distribution in the channel and only increases the curvature of the isotherm lines near the channel wall.

Streamwise velocity contours, along with the streamlines, are shown in Fig. 6. The flow conditions and roughness parameters are the same as before. The gas density decreases due to temperature increase along the channel. Therefore,

according to mass conservation law, streamwise velocity increases along the channel. Velocity variations and the curvature of the streamlines around roughness elements are shown as well in Fig. 6.

By reducing the gap between the roughness elements, the flow may be trapped in the gaps, and a vortex may appear in this region. This condition is shown in Fig. 7 for $\varepsilon = 5$, $\xi = 1$, and different values of χ. It is worth noting that although the thermal creep on the wall is the source of the fluid flow when the aspect ratio of the gap between two roughness elements falls below a specific value, bulk flow cannot penetrate this field and consequently a vortex appears there.

It can be simply shown that the aspect ratio of the gap defines as $AR = \chi - \xi$. For the cases reported in Fig. 7, the aspect ratios are $AR = 9$, 4, 3, and 2, respectively. A comprehensive analysis of the different combinations of the roughness parameters showed that no vortex would form in roughness gaps for $AR > 2$. Our previous study showed that for triangular roughness the vortex appears when $\chi = 1$ [20].
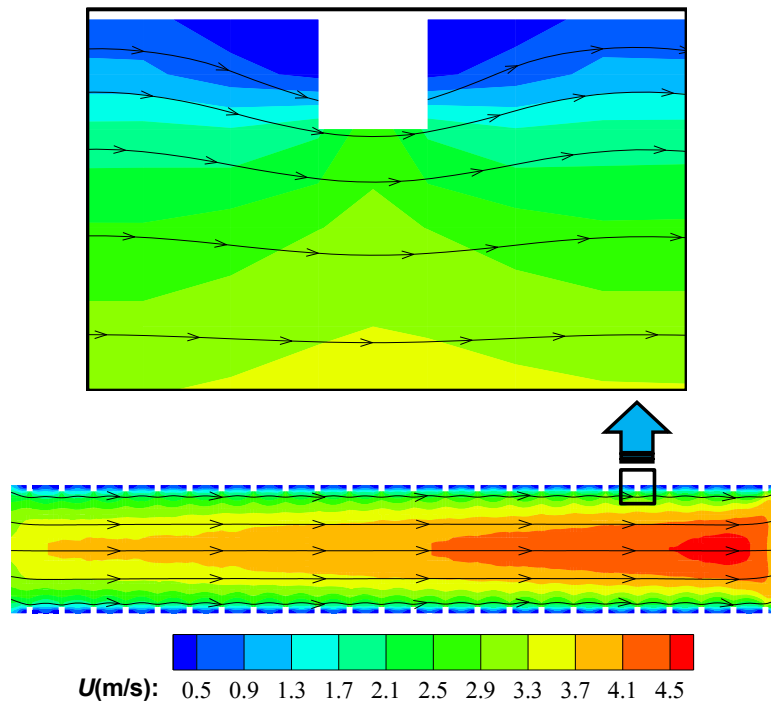
Fig. 6. Velocity contour and the stream lines along the rough microchannel
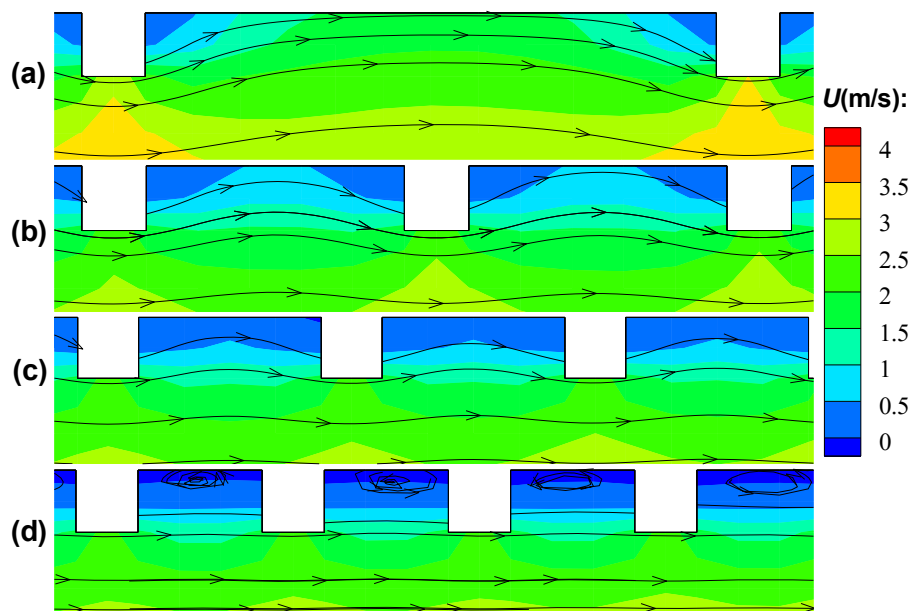

Fig. 7. Velocity contour and the streamlines around roughness elements for $\varepsilon = 5$, $\xi = 1$ and (a) $\chi = 10$, (b) $\chi = 5$, (c) $\chi = 4$, (d) $\chi = 3$
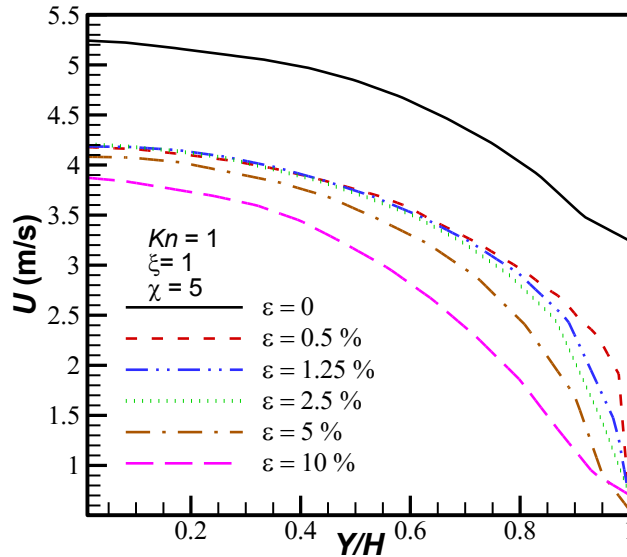
Fig. 8. Axial velocity profiles at the middle of the channel for $\xi = 1$, $\chi = 5$ and various ε

Table 2. Slip velocity and centerline velocity for $\xi = 1$, $\chi = 5$ and various ε

$\varepsilon(\%)$	$U_w \left(\frac{m}{s}\right)$	$\%$ *	$U_c \left(\frac{m}{s}\right)$	$\%$ *
0	3.25	-	5.24	-
0.5	0.97	-70	4.18	-20
1.25	0.83	-74	4.19	-20
2.5	0.77	-76	4.21	-20
5	0.59	-82	4.08	-22
10	0.72	-78	3.87	-26
	Average: -76			-21.6

* relative to smooth channel

4- 1- The effects of the relative roughness on the flow features

To study the effects of the relative roughness, various microchannels with $\xi = 1$, $\chi = 5$ and a wide range of relative roughness including $\varepsilon = 0$, 0.5, 1.25, 2.5, 5, 10% are considered, where $\varepsilon = 0$ corresponds to the smooth channel.

Fig. 8 shows the velocity profiles in the middle of the channel, $x / L = 0.5$. It can be clearly seen that the streamwise velocity in rough channels is less than a smooth channel, especially at higher relative roughnesses. It is notable that for $\varepsilon < 2.5\%$, there is no significant change in the velocity profile. For more clarification, the slip velocity

on the wall (U_w) as well as the centerline velocity (U_c), are listed in Table 2. Regardless of the relative roughness, the slip velocity for rough walls is about one order of magnitude smaller than the smooth wall. The centerline velocity is not so sensitive to relative roughness, and it is nearly constant for $\varepsilon < 2.5\%$. Although the velocity values are close together, with respect to Fig. 8 and Table 2, it is concluded that the higher ε makes lower velocity values. Therefore, increasing ε causes higher channel resistance against the thermal creep. In general, Table 2 implies that by roughening the channel
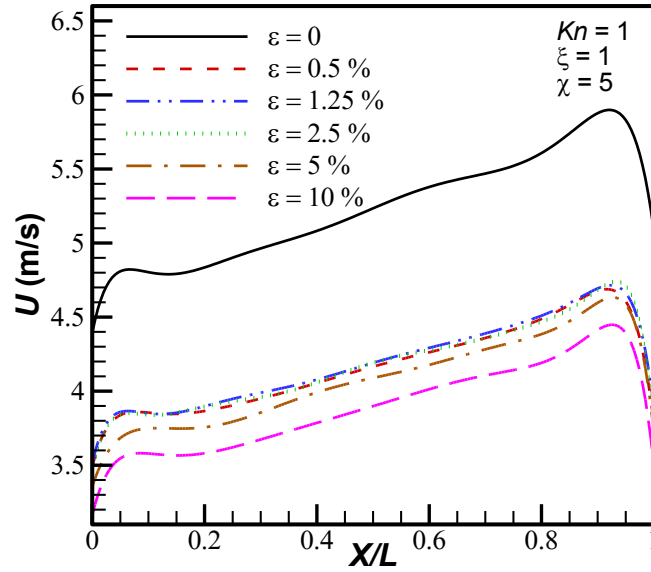
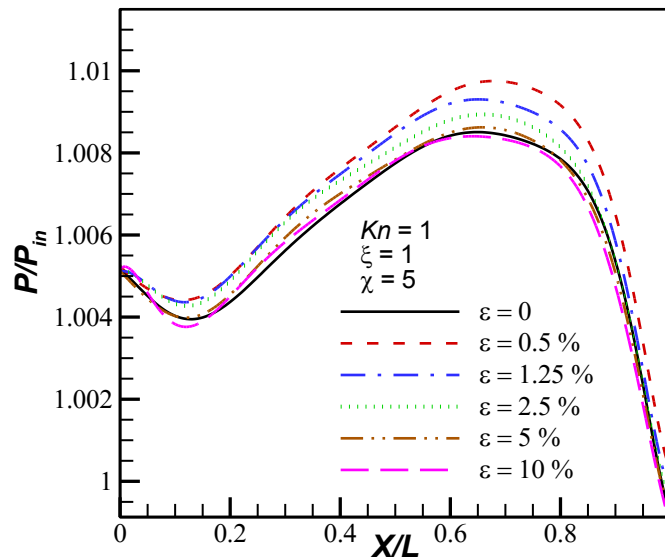**Fig. 9. Streamwise velocity component along $Y/H = 0$ for various ε**

Fig. 10. Normalized pressure distribution along channel centerline for various ε

walls, the slip velocity and the centerline velocity decrease about 76% and 21.6%, respectively.

Fig. 9 shows the streamwise velocity component along the channel centerline, $Y/H = 0$, for various values of relative roughness. This figure confirms that the flow velocity decreases with increasing the relative roughness. Besides, it is clearly seen that the flow velocity for $\varepsilon < 2.5\%$ is almost unchanged. It is noteworthy that the same behavior has been reported for triangular roughness [20].

Normalized pressure variations along the channel centerline are shown in Fig. 10 for various values of ε. This

figure depicts that there are very small variations in pressure distribution along the channel so that the difference between the inlet and outlet pressure values is only 0.6%. This behavior is also reported by Mozafari and Roohi [10]. Fig. 10 also shows that pressure distribution in smooth and rough channels is similar.

Fig. 11 represents the normalized temperature distribution along $Y/H = 0$ for various relative roughnesses. The bulk temperature approaches the wall temperature at the outlet, and so the temperature gradient is almost zero in this region. Except for the outlet, the centerline temperature distribution
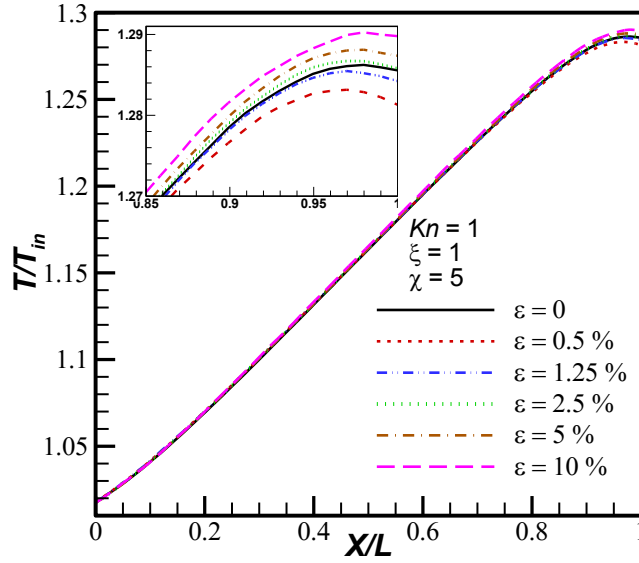
Fig. 11. Normalized temperature distribution along the channel centerline for various ε

is linear all along the channel, as was expected from a linear wall temperature boundary condition.

Since the pressure is nearly constant along with the flow, the density variation is just reversely related to the temperature, according to the equation of the state of the ideal gases. As a result, the effects of roughness parameters on the density variation can be predicted from the temperature graphs and so they are not reported here.

Mass flow rates for channels with various relative roughnesses are listed in Table 3. The mass flow rate is decreased with an increment of roughness that implies the channel resistance against the flow is increased.

The mass flow rate for the smooth channel is 2.407×10^{-7} for unit width which corresponds to inlet Reynolds number of $Re_{in} = 0.0134$. It is worth noting that the mass flow rate is reduced more than 23% as a result of a subminiature roughness of $\varepsilon = 0.5\%$; which emphasizes the importance of considering the effects of roughness in the study of thermal creep flows. Furthermore, one can generally conclude that when the relative roughness falls below 1.25%, the flow field features get independent from the size of the roughness. However, they are still very different from the smooth channel. The same conclusion has been reported for triangular roughness when $\varepsilon \leq 2.5$ [20].

4- 2- The effects of the roughness aspect ratio

The next studied parameter is the roughness aspect ratio (ξ). A microchannel having square roughness described by $\varepsilon = 5\%$, $\chi = 5$, and $\xi = 0.5, 1, 2$ at $Kn = 1$ is considered for this purpose.

The velocity profiles at cross-section $X / L = 0.5$ are plotted for various ξ in Fig. 12. As the roughness aspect ratio increases, a slight increase in velocity occurs. Actually, for a

Table 3. Slip velocity and centerline velocity for $\xi = 1$, $\chi = 5$ and various ε

$\varepsilon(\%)$	$\dot{M} \times 10^7$ (kg/s)	$\%^{*}$
0	2.407	-
0.5	1.845	-23.35
1.25	1.825	-24.18
2.5	1.782	-25.96
5	1.674	-30.45
10	1.475	-38.72

* relative to smooth channel

higher value of ξ, either the roughness length is longer or the roughness height is shorter. Anyway, the channel approaches smooth geometry, and so its resistance decreases.

The variation of Mach number along the channel centerline is plotted in Fig. 13 for various values of ξ. Regarding this figure, it can be concluded that the higher value of ξ leads to the higher Mach number, and consequently, the higher horizontal velocity along the channel.

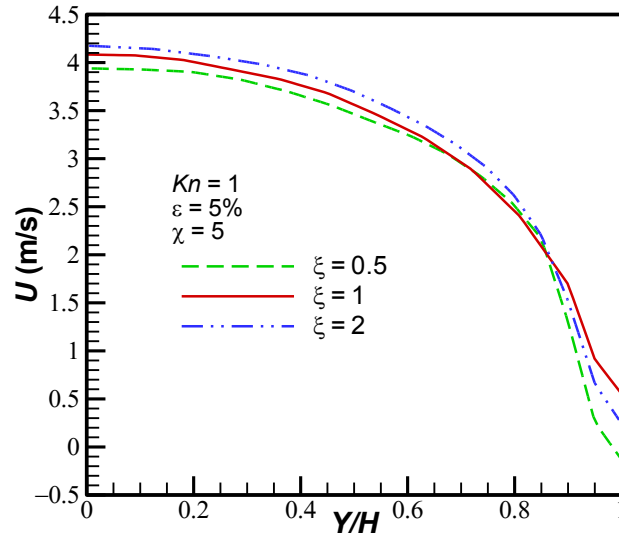The normalized pressure and temperature distribution

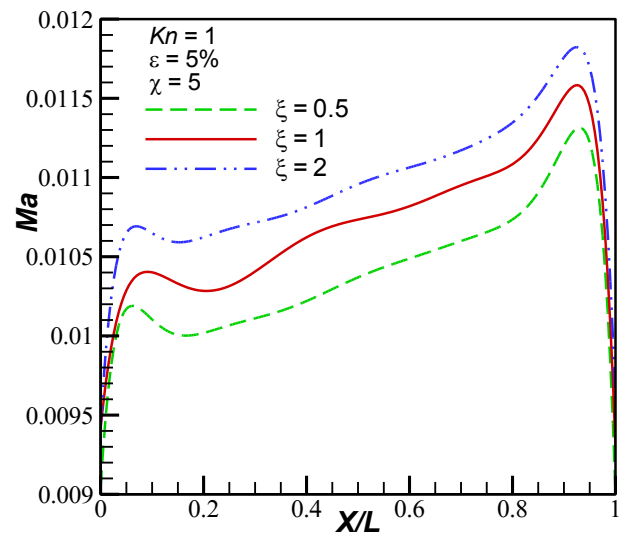**Fig. 12. Velocity profile at $X / L = 0.5$ for various ξ**

Fig. 13. Mach number distribution along $Y / H = 0$ for various ξ

along $Y / H = 0$ are shown for various values of ξ in Figs. 14 and 15, respectively. With respect to these figures, one can say that the roughness aspect ratio does not affect the centerline pressure and temperature distributions.

The channel mass flow rate is listed in Table 4 for various values of roughness aspect ratio, which indicates that the higher the value of ξ, the higher the mass flow rate. As mentioned before, the channel approaches the smooth geometry as the ξ increases, and so the channel resistance against the flow decreases. For triangular roughness, the mass flow rate slightly increases with aspect ratio, however, the aspect ratio has overally been reported to have no significant effect on the flow field [20].

4- 3- The effect of the roughness distance

The effect of the relative distance between the roughness elements (χ) is studied in this part. For this purpose, a microchannel with $\varepsilon = 5\%, \xi = 1$, and $\chi = 4$, 5, 10 is considered. Fig. 16 depicts the velocity profiles at $X / L = 0.5$ for various values of χ.

The results show that the velocity magnitude increases with the increment of χ. When the distance between the roughness elements increases, the number of the elements per unit length reduces, and consequently, the channel approaches the smooth geometry. Therefore as Fig. 16 shows, the velocity magnitude increases with the increment of χ. Notably, the velocity profile is not affected by χ when
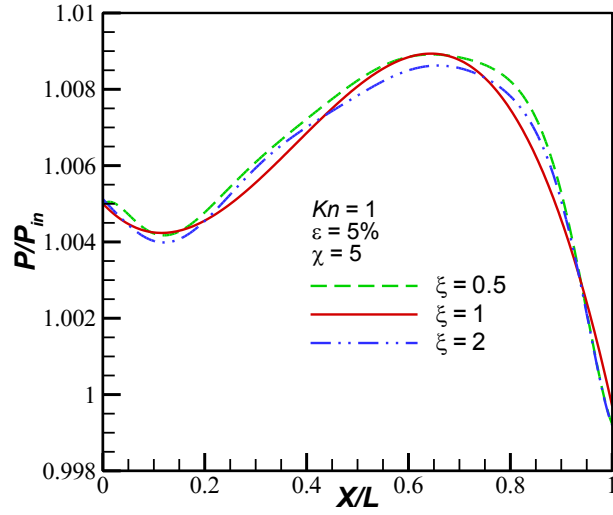
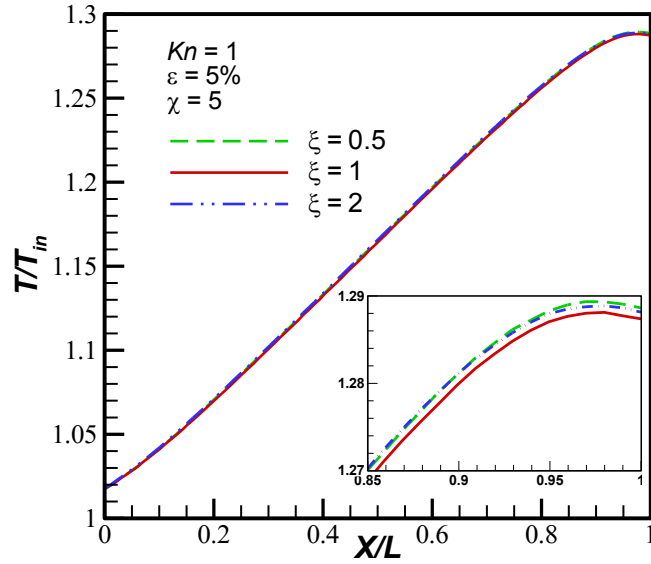**Fig. 14. Normalized centerline pressure distribution for various** ξ

Fig. 15. Normalized centerline temperature distribution for various ξ

Table 4. Mass flow rate for various values of ξ

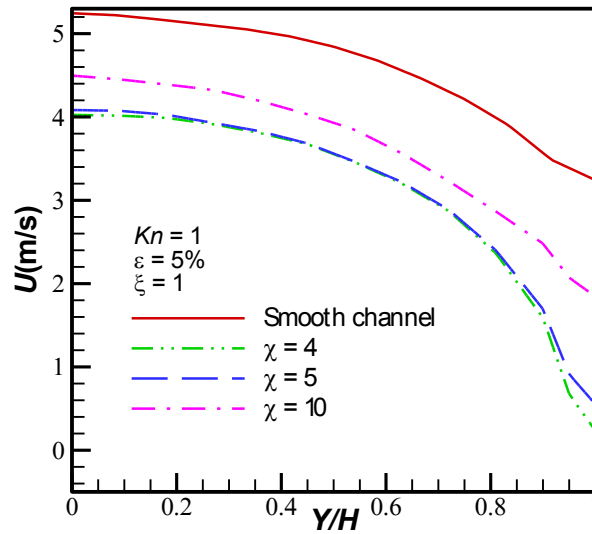| ξ	$\dot{M} \times 10^7$ (kg/s)	% *
Smooth Channel	2.407	-
0.5	1.599	-33.6
1	1.674	-30.5
2	1.701	-29.3

* relative to smooth channel

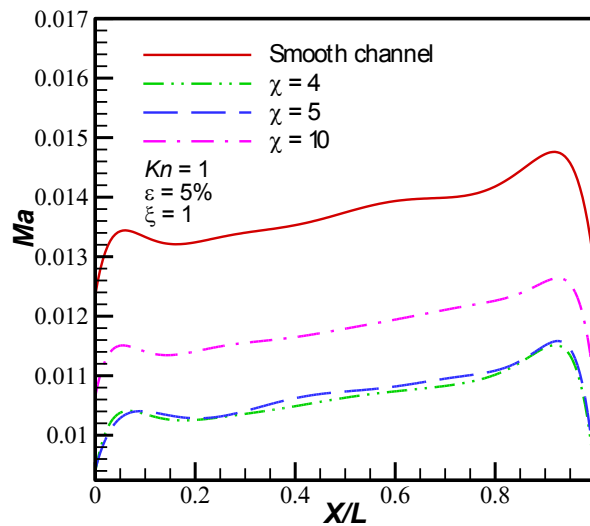Fig. 16. The velocity profile at $X/L = 0.5$ for various χ

Fig. 17. Mach number variations along $Y/H = 0$ for various χ

$\chi \le 5$. Mach number variation along the channel centerline is plotted in Fig. 17 for different values of χ. Regarding this figure, it is clear that the curves almost coincide with each other for $\chi \le 5$.

The effects of variation of χ on the normalized centerline pressure and temperature distribution are shown in Figs. 18 and 19, respectively. As can be seen, the variation of χ does not affect the centerline pressure and temperature distributions.

The channel mass flow rate is listed in Table 5 for different values of χ. With the increase of χ, and subsequently decrement of channel resistance against the flow, the mass flow rate is increased. The results presented in this subsection indicate that the flow field features are independent of the distance between roughness elements when $\chi \le 5$. The same conclusion has been reported for triangular roughness when $\chi \le 3$ [20].

4- 4- The impact of the shape of the roughness
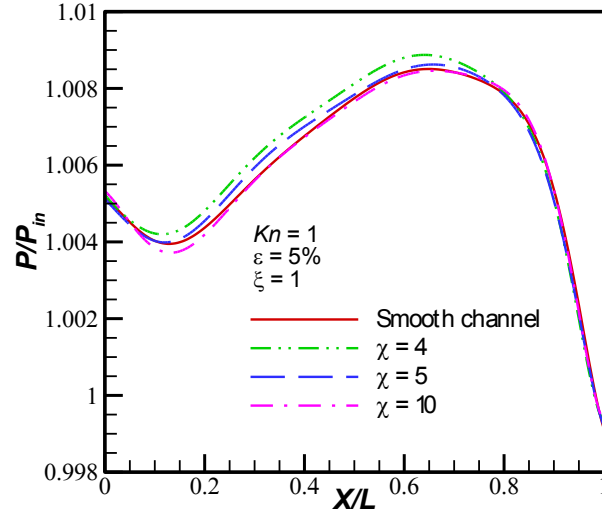
Since the micro/nano flows have memory [21], they are

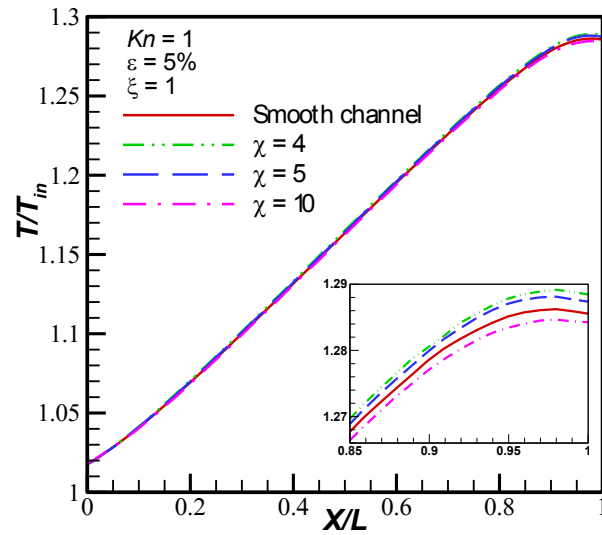**Fig. 18. Normalized pressure variations along** $Y/H = 0$ **for various** χ

Fig. 19. Normalized temperature variations along $Y/H = 0$ **for various** χ

geometry-dependent. Comparing the present work with our previous paper on triangular roughness [20], the sensitivity of flow parameters to the roughness shape is emphasized. The most important differences between these two studies are summarized in Table 6.

5- Conclusion

The effects of roughening the micro/nanochannels on the flow induced by the thermal creep phenomenon in Knudsen pumps are studied in this paper. Direct Simulation Monte Carlo method is used to simulate the thermal creep flow in the transient flow regime. For this purpose, dsmcFoamStrath solver of the open-source package, OpenFOAM, is utilized.

Table 5. Mass flow rate for various values of χ

χ	$\dot{M} \times 10^7$ (kg/s)	% *
smooth channel	2.407	-
4	1.649	-31.5
5	1.674	-30.5
10	1.918	-20.3

* relative to smooth channel

Table 6. Comparison of this work with triangular roughness study [20].

Parameter	Triangular roughness [20]	Square roughness	Comparison
Roughness surface along the core flow	Two oblique sides	One parallel side	Having a side parallel to the main flow, the squared roughness has less resistance against the mainstream.
Validation	Validated by pressure-driven flow at $Kn = 0.078$	Validated by shear-driven flow at $Kn = 0.08$	Thermal creep flow is somehow similar to shear-driven flow in which the fluid motion originates from the wall. So, in this work Couette flow was used for validation.
Vortex formation	Appeared when the roughness elements connect to each other	Appears when the gap aspect ratio is $AR < 2$	In this study, many roughness configurations (various ε, ξ and χ) were investigated and a criterion for vortex formation was obtained.
Relative roughness range	$\varepsilon \geq 1.25$ are considered	$\varepsilon \geq 0.5$ are considered	Unlike in triangular roughness where the flow was nearly the same for $\varepsilon \leq 2.5$, this study showed that for squared roughness this criterion decreases to $\varepsilon \leq 1.25$. The mass flow rate in square roughness is greater than in triangular roughness. For example at $\varepsilon = 1.25$ the mass flow rates are 1.825E-7 and 1.785E-7 kg/s for squared and triangular roughnesses, respectively.
Impact of roughness aspect ratio	In general, it has no significant effect	Affects flow characteristics	This study showed that when the roughness element has a side along the main flow, the roughness aspect ratio affects the flow features.
Impact of roughness distance	Has no effect when $\chi \leq 3$	Has no effect when $\chi \leq 5$	This study showed that the flow features are less sensitive to roughness distance in the squared roughness. Note that usually $\chi \leq 5$.

The roughness was considered as square bumps described by the height of the elements, distance between two successive elements, and the aspect ratio of them. These parameters are studied in a wide range of $0 < \varepsilon < 10$, $0.5 < \xi < 2$, and $3 < \chi < 10$. The summary of the significant results is presented below:

The velocity profile of the thermal creep flow is parabolic, whose shape becomes flattered as the thermal creep gets stronger.

If the gap is small enough ($AR \leq 2$), a vortex will appear between successive roughness elements. In this situation, the roughness elements lie in a sublayer flow.

The existence of the roughness elements has no significant effect on the temperature distribution inside the channel, and the temperature gradient is linear in the distance far from the inlet and outlet of the channel.

In general, the slip velocity on the walls and centerline velocity have a reduction of about 76% and 22%, respectively, in comparison with the smooth channel.

In the presence of the roughness, no matter how small, the flow features relative to the smooth channel experience significant variation, e.g., the subminiature roughness of $\varepsilon = 0.5\%$ results in a decrease in the mass flow rate. Interestingly, the flow field features are independent of the relative roughness for $\varepsilon \leq 1.25\%$.

By increasing the relative roughness, the channel resistance against the thermal creep flow increases, and consequently, the velocity and mass flow rate decrease. The mass flow rate decrease by about 20% when the relative roughness increases from 0.5 to 10.

The flow field features are independent of the roughness distance for $\chi \leq 5$.

Nomenclature

a, b, c	Roughness geometrical dimensions, m
AR	Gap aspect ratio
c_r	Magnitude of pre-collision relative velocity
d	Nitrogen molecular diameter, m
f_{num}	The ratio of number of real molecules to simulated particles
g_{ij}	relative velocity, m/s
H	Half of channel height, m
K	Boltzmann constant, $1.38064852 \times 10^{-23}$ J/K
Kn	Knudsen number
m	Nitrogen molecular mass, kg
$\dot{M}$	Mass flow rate, kg/s
Ma	Mach number
N_c	number of collisions in each cell
N^l	Number of particles in cell l
P	Pressure, Pa
p_{ij}	probability of collision
R	Specific gas constant, J/kg.K
Re	Reynolds number
T	Temperature, K
U	Streamwise velocity component, m/s
u, v, w	Velocity components, m/s
$\forall$	Cell volume, m^3
X, Y	Cartesian axes with the origin at the channel centerline, m

Greek symbols

Δt	DSMC time step, s
ε	relative roughness
ε	Space collision angle, rad
λ	Mean free path, m
ξ	roughness aspect ratio
σ_{ij}	Collision cross-section, m^2
χ	roughness distance
χ	Angle of deflection, rad

Subscript

c	channel centerline
mp	most probable
r	pre-collision relative parameter
w	wall

References

[1] H. Yamaguchi, G. Kikugawa, Molecular dynamics study on flow structure inside a thermal transpiration flow field, Physics of Fluids, 33(1) (2021) 012005.

[2] S.E. Vargo, E.P. Muntz, Initial results from the first MEMS fabricated thermal transpiration-driven vacuum pump, AIP Conference Proceedings, 585(1) (2001) 502-509.

[3] N.K. Gupta, Y.B. Gianchandani, A planar cascading architecture for a ceramic Knudsen micropump, in: TRANSDUCERS 2009 - 2009 International Solid-State Sensors, Actuators and Microsystems Conference, Denver, CO, 2009, pp. 2298-2301.

[4] N.V. Toan, N. Inomata, N.H. Trung, T. Ono, Knudsen pump produced via silicon deep RIE, thermal oxidation, and anodic bonding processes for on-chip vacuum pumping, Journal of Micromechanics and Microengineering, 28(5) (2018) 055001.

[5] K. Kugimoto, Y. Hirota, Y. Kizaki, H. Yamaguchi, T. Niimi, Performance prediction method for a multi-stage Knudsen pump, Physics of Fluids, 29(12) (2017) 122002.

[6] J. Ye, J. Shao, J. Xie, Z. Zhao, J. Yu, Y. Zhang, S. Salem, The hydrogen flow characteristics of the multistage hydrogen Knudsen compressor based on the thermal transpiration effect, International Journal of Hydrogen Energy, 44(40) (2019) 22632-22642.

[7] K. Aoki, P. Degond, L. Mieussens, M. Nishioka, S. Takata, Numerical Simulation of a Knudsen Pump Using the Effect of Curvature of the Channel, in: Rarefied Gas Dynamics, Novosibirsk, 2007, pp. 1079-1084.

[8] D.M. Bond, V. Wheatley, M. Goldsworthy, Numerical investigation of curved channel Knudsen pump performance, International Journal of Heat and Mass Transfer, 76 (2014) 1-15.

[9] D.M. Bond, V. Wheatley, M. Goldsworthy, Numerical investigation into the performance of alternative Knudsen pump designs, International Journal of Heat and Mass Transfer, 93 (2016) 1038-1058.

[10] M.S. Mozaffari, E. Roohi, On the thermally-driven gas flow through divergent micro/nanochannels, International Journal of Modern Physics C, 28(12) (2017) 1750143.

[11] G. Tatsios, G. Lopez Quesada, M. Rojas-Cardenas, L. Baldas, S. Colin, D. Valougeorgis, Computational investigation and parametrization of the pumping effect in temperature-driven flows through long tapered channels, Microfluidics and Nanofluidics, 21(5) (2017) 99.

[12] B.-Y. Cao, M. Chen, Z.-Y. Guo, Effect of surface roughness on gas flow in microchannels by molecular dynamics simulation, International Journal of Engineering Science, 44(13) (2006) 927-937.

[13] C. Zhang, Y. Chen, Z. Deng, M. Shi, Role of rough surface topography on gas slip flow in microchannels, Physical Review E, 86(1) (2012) 016319.

[14] O.I. Rovenskaya, G. Croce, Numerical simulation of gas flow in rough microchannels: hybrid kinetic–continuum approach versus Navier–Stokes, Microfluidics and Nanofluidics, 20(5) (2016) 81.

[15] J. Jia, Q. Song, Z. Liu, B. Wang, Effect of wall roughness

on performance of microchannel applied in microfluidic device, Microsystem Technologies, 25(6) (2019) 2385-2397.

[16] X. Wang, T. Su, W. Zhang, Z. Zhang, S. Zhang, Knudsen pumps: a review, Microsystems & Nanoengineering, 6(1) (2020) 26.

[17] [17] K. Yamamoto, H. Takeuchi, T. Hyakutake, Effect of Surface Grooves on the Rarefied Gas Flow Between Two Parallel Walls, AIP Conference Proceedings, 762(1) (2005) 156-161.

[18] J. Shao, J. Ye, Y. Zhang, S. Salem, Z. Zhao, J. Yu, Effect of the microchannel obstacles on the pressure performance and flow behaviors of the hydrogen Knudsen compressor, International Journal of Hydrogen Energy, 44(40) (2019) 22691-22703.

[19] J. Ye, J. Shao, Z. Hao, S. Salem, Y. Zhang, Y. Wang, Z. Li, Characteristics of thermal transpiration effect and the hydrogen flow behaviors in the microchannel with semicircular obstacle, International Journal of Hydrogen Energy, 44(56) (2019) 29724-29732.

[20] N. Mirnezhad, A. Amiri-Jaghargh, The study of the effects of triangular roughness on the thermal creep flow in Knudsen pumps with DSMC method, Journal of Solid and Fluid Mechanics, 10(4) (2020) 97-109.

[21] G.E. Karniadakis, A. Beskok, N. Aluru, Microflows and Nanoflows: Fundamentals and Simulation, Springer-Verlag New York, 2005.

[22] W. Wagner, A convergence proof for Bird's direct simulation Monte Carlo method for the Boltzmann equation, Journal of Statistical Physics, 66(3) (1992) 1011-1044.

[23] G.A. Bird, Molecular Gas Dynamics and the Direct Simulation of Gas Flows, Clarendon Press, 1994.

[24] A. Amiri-Jaghargh, E. Roohi, H. Niazmand, S. Stefanov, DSMC Simulation of Low Knudsen Micro/Nanoflows Using Small Number of Particles per Cells, Journal of Heat Transfer, 135(10) (2013).

[25] A. Amiri-Jaghargh, E. Roohi, S. Stefanov, H. Nami, H. Niazmand, DSMC simulation of micro/nano flows using SBT–TAS technique, Computers & Fluids, 102 (2014) 266-276.

[26] W.W. Liou, Y.C. Fang, Implicit Boundary Conditions for Direct Simulation Monte Carlo Method in MEMS Flow Predictions, Computer Modeling in Engineering \& Sciences, 1(4) (2000) 119--128.

[27] T. Ohwada, Y. Sone, K. Aoki, Numerical analysis of the shear and thermal creep flows of a rarefied gas over a plane wall on the basis of the linearized Boltzmann equation for hard-sphere molecules, Physics of Fluids A: Fluid Dynamics, 1(9) (1989) 1588-1599.

[28] H. Akhlaghi, E. Roohi, Mass flow rate prediction of pressure–temperature-driven gas flows through micro/nanoscale channels, Continuum Mechanics and Thermodynamics, 26(1) (2014) 67-78.

[29] F.J. Alexander, A.L. Garcia, B.J. Alder, Cell size dependence of transport coefficients in stochastic particle algorithms, Physics of Fluids, 10(6) (1998) 1540-1542.

[30] N.G. Hadjiconstantinou, Analysis of discretization in the direct simulation Monte Carlo, Physics of Fluids, 12(10) (2000) 2634-2638.